Developmental Cell, Volume *22*

Supplemental Information

Dorsal-Ventral Gene Expression in the *Drosophila* Embryo Reflects the Dynamics and Precision of the Dorsal Nuclear Gradient

Gregory T. Reeves, Nathanie Trisnadi, Thai V. Truong, Marcos Nahmad, Sophie Katz, and Angelike Stathopoulos

Supplemental Inventory

Supplemental Figure Legends:

Supplemental Experimental Procedures:

Supplemental References

Figure S1

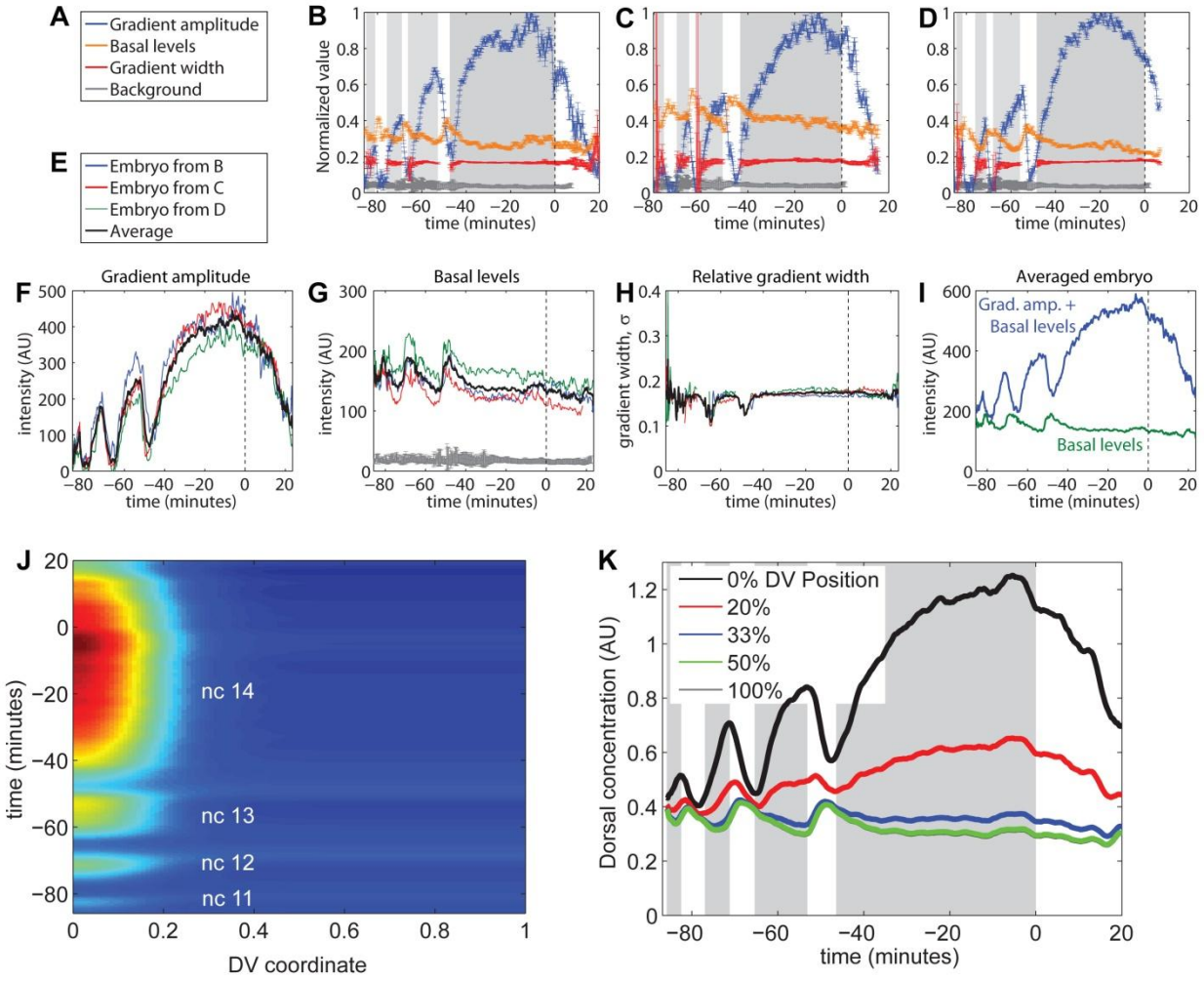

Figure S1: Measurements and averaging of three live embryos. Related to Figure 3. (A) Legend for plots in B-D. (B-D) Plots of the gradient amplitude, basal levels, and gradient width (interphase only) of Dorsal-Venus from three separate live embryos. Embryo in B was analyzed for Figure 3D-I. The gray curve at the bottom represents the background levels, which is the intensity of the Venus channel in a control embryo carrying H2A-RFP only. The background levels should be compared to the basal levels and not to the gradient amplitude or width. Errorbars denote 68% confidence intervals on the fitted parameters. (E) Legend for plots in F-H. (F) Plot of gradient amplitudes of the three embryos with the durations of the interphases and

mitoses aligned. The black curve represents the average of the three embryos. (G) Same as F except with basal levels. The gray curve at the bottom is the background levels from the control embryo. (H) Same as F except with the gradient width. (I) Averaged basal levels (green) and gradient amplitude plus basal levels (blue). (J) Heatmap of Dorsal nuclear levels over time and space averaged from three live embryos. (K) Traces of averaged Dorsal concentration seen by nuclei at five different DV locations.

Figure S2

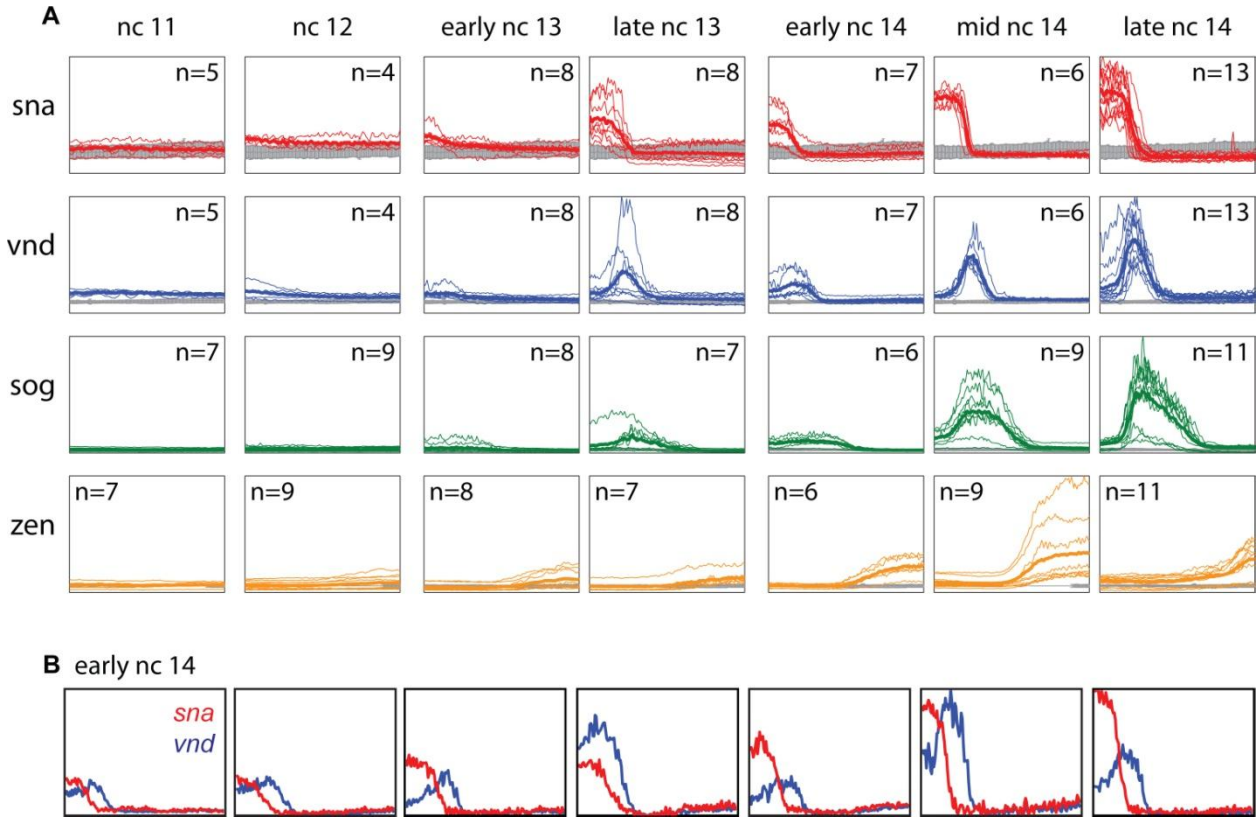

Figure S2: Profile overview of Dorsal target genes. Related to Figure 4. (A) Overlay of individual profiles for each Dorsal target gene at each nuclear cycle, with the thicker line representing the average and *n* being the number of embryos analyzed. Gray curves represent background levels specific to the mRNA antibody and channel (error bars standard deviation; see Supplemental Experimental Procedures). (B) Profiles of individual embryos at early nc 14 co-stained with *sna* (red) and *vnd* (blue) show a large range in intensity and pattern even within a nuclear cycle substage.

Figure S3

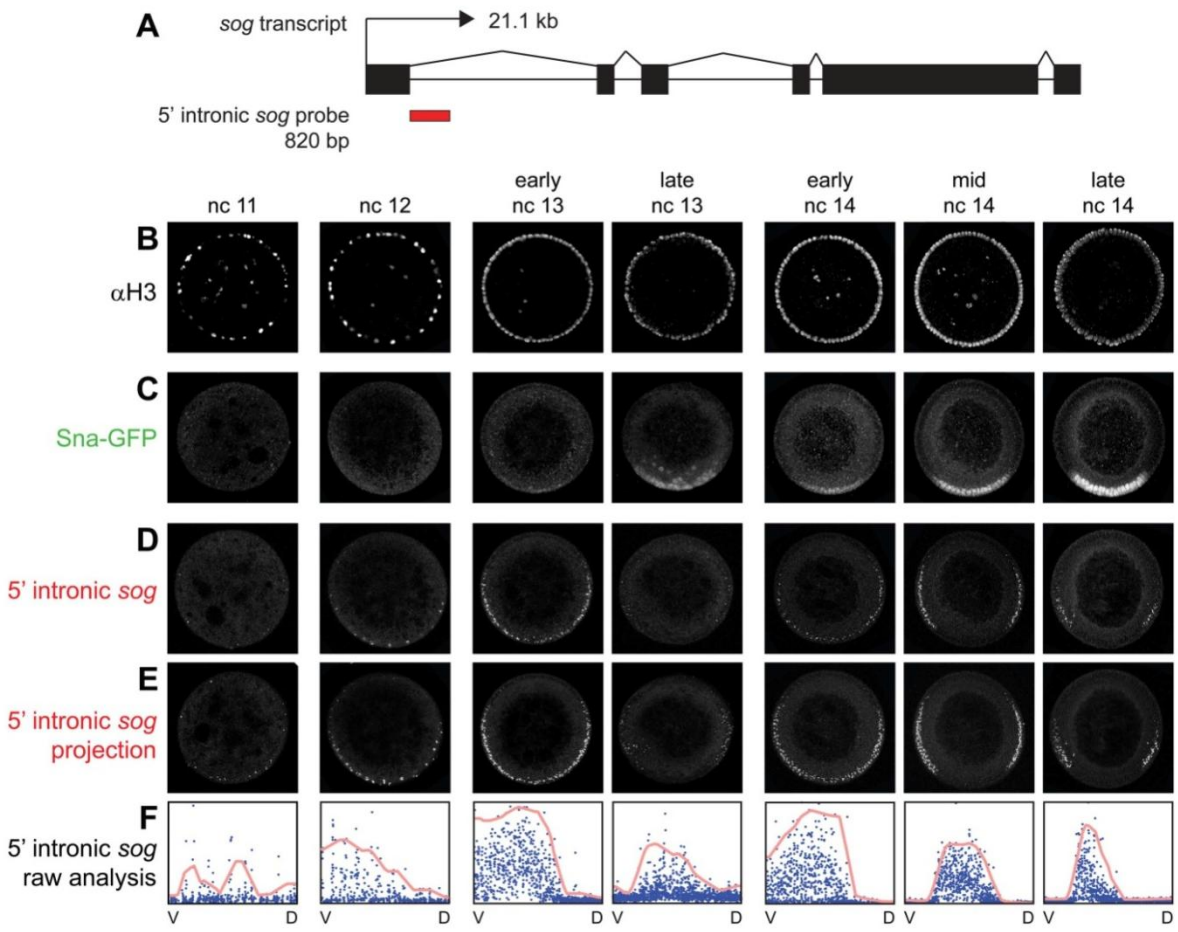

Figure S3: Cross-sections of embryos with Sna-GFP and intronic *sog*. Related to Figure 5. (A) The 21.1 kb *sog* transcript contains 6 exons and 5 introns. The 820 bp intronic *sog* probe used in this study starts at the beginning of the first intron (red bar). (B) 1.3 micron optical slices of embryos containing the Sna-GFP transgene are shown stained with nuclear Histone H3. (C) The same embryo for each stage was also stained with anti-GFP for the Sna-GFP protein. (D) Same embryo from B and C except with intronic *sog*. (E) The 19.5 micron z-stack projection is displayed to fully capture the intronic *sog* expression. (F) Raw analysis of the single embryos shown in B-E with blue dots representing intronic *sog* and its corresponding profile curve in pink. Analyses of additional embryos are shown in Figure 5G-J. D: dorsal, V: ventral.

Figure S4

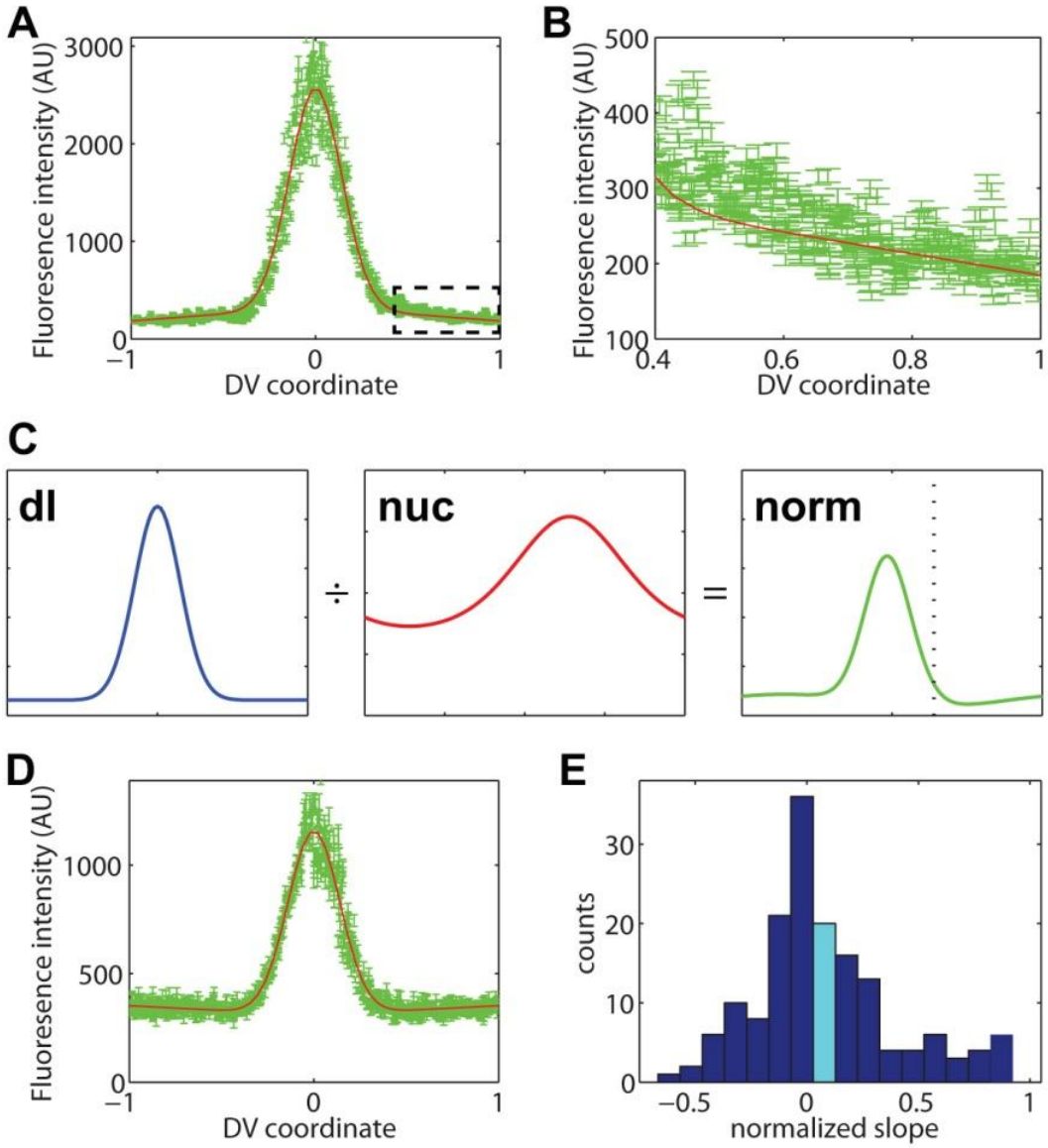

Figure S4: Detecting the slope of the gradient tail. Related to Figure 6. (A) Dorsal nuclear gradient for a representative embryo (with normalized gradient tail slope = -0.06). Outside the Gaussian regime, the tail appears to slope gradually downward in a shallow linear fashion. Dashed box represents the portion of this plot that is depicted in part B. Error bars denote the standard error of the intensity of the pixels in each nucleus (also in B,D). (B) Same embryo from A, but zoomed-in on the tail. While the tail could be described by other functions, it is shallow

enough such that a one-term Taylor expansion is sufficient. (C) Scheme of numerical controls to show that the slope of the gradient tail is, on average, negative. The blue curve is a hypothetical Dorsal gradient assuming the tail is flat. The red curve is a possible non-uniformity in the intensity of the nuclei, based on real images. The peak of this curve has been randomly placed with respect to the peak in the Dorsal gradient (i.e., the presumptive ventral midline). When the Dorsal gradient is normalized by the nuclear intensity (green curve), artificial x-dependence emerges. Dotted line: random placement of the peak of nuclear intensity. (D) Embryo (real data) in which gradient tail slope is positive. (E) Histogram of simulated gradient tail slopes. The mean is 0.08 with a 95% confidence interval of the mean of [0.03, 0.13].

Figure S5

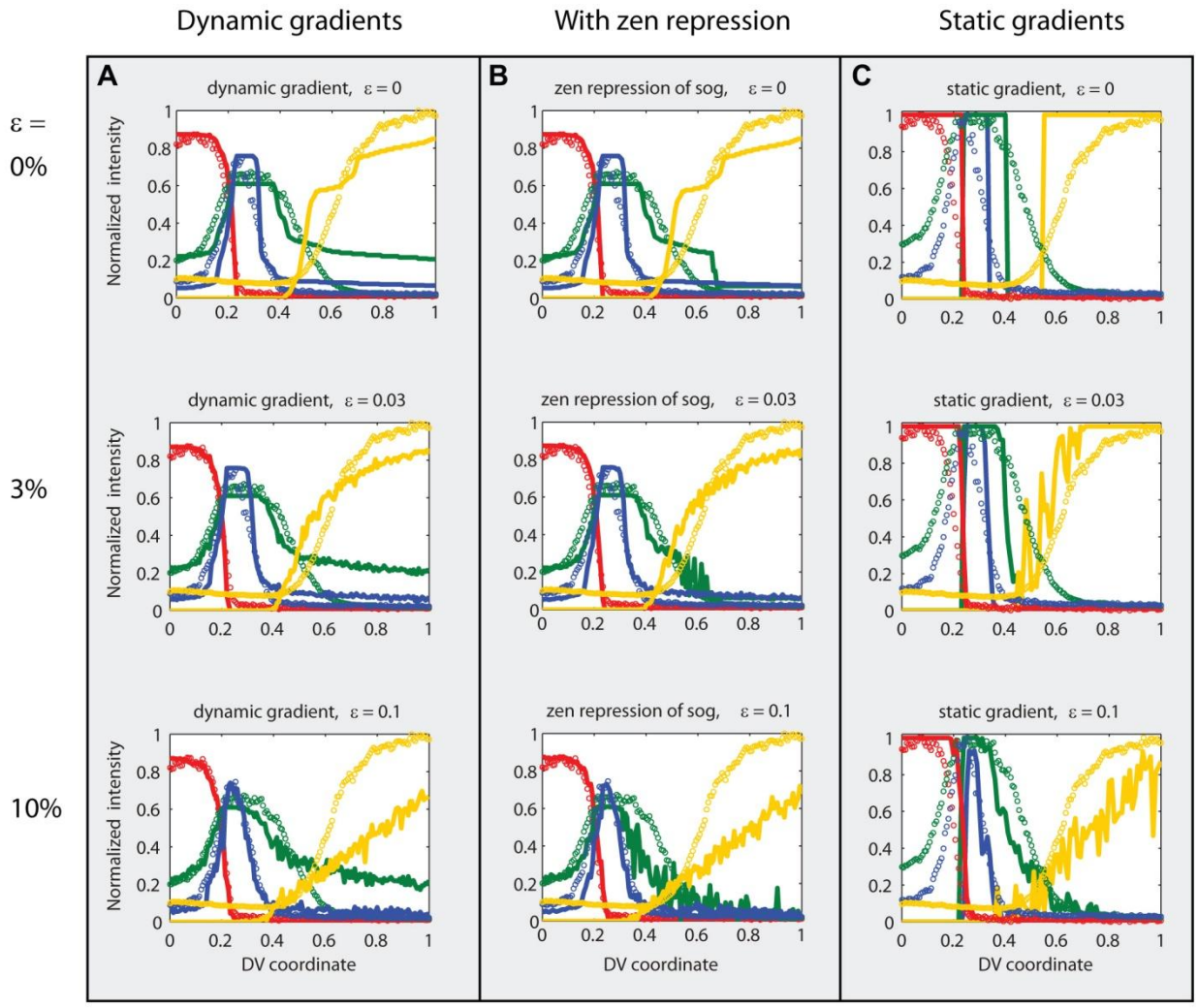

Figure S5: Simulations of mRNA patterns resulting from dynamic and static Dorsal gradients and different levels of stochastic noise. Related to Figure 7. In this figure, the noise level, ϵ , was varied to determine the effect this parameter had on the mRNA patterns. (A) In dynamic gradients, little effect was found for the Type I and II genes, but the graded response of the Type III genes was affected. In general, too much noise was adverse. However, even without noise, the Type III genes maintained graded borders. This demonstrates that the basal levels decreasing may be one factor that contributes to graded mRNA patterns. (B) When

repression of *sog* by *zen* is included, the graded dorsal expression of *sog* better matches observed patterns indicating the possibility of a repressor. (C) In static gradients, some small amount of noise is essential for creating graded patterns, but too much noise was adverse. This demonstrates that a noisy gradient tail and time-averaging may be one factor that contributes to the graded patterns of Type III genes. Shown are the late nc 14 Dorsal target genes *sna* (red), *vnd* (blue), *sog* (green), and *zen* (yellow). Circles denote averages of fluorescent in situ hybridization patterns from > 10 embryos, and solid curves denote simulation results.

Supplemental Experimental Procedures

Primers used

Dorsal homology arms
dl LA-AscI-F: AGGCGCGCCCGCTGCTGATATGATGGTTG
dl-LA-BamHI-R: CGCGGATCCGATTTGTCCAGAAACCTGTG
dl-RA-BamHI-F: CGAGGTAATTTTTAATGGATCCTGCC
dl-RA-AsiSI-R: AAGGAAAAAAGCGATCGCCTGGAACTGTGTCTTTATC
GalK primers
Dorsal-GalK-F: TGCGC CTC AAT TCG GAA GAT CTG CAG ATA TCG AAC CTG TCC ATA TCC ACG GAA GGA GGC GGT GGG GGT CCT GTT GAC AAT TAA TCA TCG GCA
Dorsal-GalK-R: CT ACT GAC TCC TCC GTT CTT GCT CTG CTC TGG TTC GTT GTG AAA AAG GTA TCA GCA CTG TCC TGC TCC TT
Venus insertion and adding 6XGly
Dorsal-Venus-F: TGCGC CTC AAT TCG GAA GAT CTG CAG ATA TCG AAC CTG TCC ATA TCC ACG GAA GGA GGC GGT GGG GGTATGGTGAGCAAGGGCGAGGA
Dorsal-Venus-R: CTACTGACTCCTCCGTTCTTGCTCTGCTCTGGTTCGTTGTGAAAAAGGTA CTTGTACAGCTCGTCCATGCCC
GFP insertion and adding 6XGly
dl-GFP-F: TGCGC CTC AAT TCG GAA GAT CTG CAG ATA TCG AAC CTG TCC ATA TCC ACG GAA GGA GGC GGT GGG GGT ATGAGCAAGGGCGAGGAACT
GFP insertion with SV40 terminator
dl6xglyGFP-f: CTCAATTCGGAAGATCTGCAGATATCGAACCTGTCCATATCCACGGAAGGAGGC GGTGGGGGTATGAGCAAGGGCGAGGAACT
dlGFPkan-r: TCATATCATCATCCTACTGACTCCTCCGTTCTTGCTCTGCTCTGGTTCGTTGTGAA AAAGGTATCGAAGAGCTATTCCAGAAGTAGTGA

Dorsal-fluorescent protein fusions

Two slightly different *dorsal-GFP* constructs were used in this study. The *dorsal-GFP* construct used for live in vivo imaging was cloned analogous to *dorsal-venus*, except this first *dorsal-GFP* created contains an additional terminator sequence, SV40 following the *gfp* gene. Therefore, the construct was remade as a seamless insertion of *gfp* into the *dorsal* locus (similar to how *dorsal-venus* was constructed) to produce a seamless version: *dorsal-gfp* (seamless). Nevertheless, fixed analysis of *dorsal-GFP* (seamless) showed that even this construct supported

a dorsal gradient that was wider than that supported by *dorsal-venus*. Thus, the wider gradient associated with *dorsal-gfp* is not due to the SV40 terminator sequence. Moreover, both *dorsal-GFP* (seamless) and *dorsal-GFP* (which contains the SV40 terminator sequence) require two copies to rescue the *dl* mutant, unlike *dorsal-venus*, which complements at one copy. These GFP constructs have significantly larger widths compared to wildtype and Dorsal-Venus [Fig. 1F, *dl-GFP* (live) and *dl-GFP* seamless (fixed)].

In addition, the Dorsal-Venus protein has the following sequence associated with its C-terminus (from the *dorsal* gene 3'UTR before reaching a stop codon): YLFHNEPEQSKNGGVSRMMI.

Sna-GFP fly stock

Analysis of the Snail protein was done through antibody staining of GFP in transgenic embryos containing a 25 kb Sna-GFP rescue transgene previously described (Dunipace et al., 2011). This construct includes the endogenous 3' UTR as well as an SV40 terminator sequence associated with the GFP insertion, and importantly is able to complement *sna* mutants. More information can be found in Dunipace et al., 2011.

Embryo antibody stainings

We performed double in situ and antibody fluorescent stainings using standard protocols but eliminated Proteinase K treatment (Kosman et al., 2004). Antisense RNA probes were made against *sna, vnd, sog, 5' intronic sog, zen, ths,* and *Neu3*. Primary antibodies used are anti-Dorsal 7A4 monoclonal mouse (DSHB), anti-GFP polyclonal goat (Rockland 600101215) for GFP and Venus detection, anti-Histone H3 polyclonal rabbit (Abcam 1791), anti-DIG mouse (Roche

11333062910), anti-FITC goat (Rockland 600101096), and anti-BIO goat (Rockland 600101098). Secondary antibodies from Invitrogen used are Alexa Fluor 488 anti- goat (11055), Alexa Fluor 555 anti- goat (21432) and mouse (31570), and Alexa Fluor 647 anti- rabbit (21245).

Image analysis

For optical sections of embryos, the perimeter of the embryo was found based on the local drop in intensity in the radial direction for 60 points equally-spaced in the azimuthal angle, similar to the method described in Liberman et al., 2009. To detect gene expression, first 300 equally-spaced points were placed around the perimeter of the embryo, interpolating from the original 60 points. Second, a series of quadrilaterals was defined by two adjacent points on the perimeter and two corresponding points 20 microns closer to the center of the embryo. The intensity of gene expression at each point around the perimeter of the embryo was computed as the mean fluorescence intensity inside each quadrilateral.

Nuclei were detected in the following manner. First, the nuclear layer was unrolled to 20 microns deep into the embryo, transforming the annular nuclear layer into a strip, as described previously (Liberman et al., 2009). The fluorescent intensity was averaged along the radial axis of the embryo to give a 1D approximation to the nuclear layer. This 1D approximation was morphologically opened using a line of width 3 microns, and boundaries between adjacent nuclei were determined based on a watershed algorithm. Rectangles in the strip of nuclei were defined by the locations of these boundaries, and within each rectangle the raw nucleus was segmented using a best-fit threshold protocol (Otsu, 1979). To eliminate spurs and feathers, each raw nucleus was morphologically opened using a disk of radius 1.5 microns, yielding a final set of nuclei in the strip of the nuclear layer. The locations of each “on” pixel in the strip were then

transformed back into the original 2D embryo image, maintaining the distinction between neighboring nuclei. In live embryos, this segmentation algorithm was used for nc 13 and 14. For nc 11 and 12, nuclei were detected by choosing the center of the nucleus manually. Each of the manually-detected nuclei were then taken to be a disc, 4.4 microns in diameter, centered at this point.

After detection of the nuclei, the Dorsal nuclear gradient was calculated based on previous methods (Liberman et al., 2009). Briefly, the Dorsal gradient concentration in each nucleus was the average intensity of the Dorsal channel for that nucleus divided by the average intensity of the histone channel for that nucleus, multiplied by the mean intensity of all of the nuclei. Nuclear Sna-GFP intensities were calculated in a similar manner.

Characterizing the Dorsal gradient

Each measurement of the Dorsal gradient was fit to either Eqn. 1 (all embryos besides Figure 6) or Eqn. 2 (embryos depicted in Figure 6), with the x^2 term replaced by $(x-\mu)^2$, where μ is the unknown location of the ventral midline. Matlab's curve-fitting function "fit" was used, using nonlinear least squares and the following starting guesses: for gradient amplitude, the difference between the maximum intensity nucleus and the minimum intensity nucleus; for basal levels, the minimum intensity nucleus; for the location of the ventral midline, the location of the highest intensity nucleus; for the width of the gradient, 0.15; for the slope of the tail (where applicable), zero. The following lower bounds on parameters were used: for gradient amplitude, one-tenth the difference between the maximum intensity nucleus and the minimum intensity nucleus; for basal levels, zero; for the location of the ventral midline, the location of the highest intensity nucleus minus 30% DV location; for the width of the gradient, 0.05; for the slope of the

tail (where applicable), -10^6. The following upper bounds on parameters were used: for gradient amplitude, ten times the difference between the maximum intensity nucleus and the minimum intensity nucleus; for basal levels, the average between the maximum intensity nucleus and the minimum intensity nucleus; for the location of the ventral midline, the location of the highest intensity nucleus plus 30% DV location; for the width of the gradient, 1; for the slope of the tail (where applicable), 10^6. Uncertainties in parameter estimates were taken to be one-half the width of the 68% confidence interval. In particular, the uncertainties in locating the ventral midline of each embryo in Fig. 6A were all less than 1% of the DV axis length.

To normalize the Dorsal nuclear gradients in fixed embryos (Fig. 6A), the raw Dorsal nuclear gradient for embryo *i* was subtracted by B_i, then was divided by A_i, where A_i, B_i are the gradient amplitude and basal levels for embryo *i*, respectively. After aligning each of the embryos to their individual ventral midlines (calculated as described above) and normalizing in this fashion, the embryos in Fig. 6A were plotted on top of each other.

Simulations of gradient tail slopes

The histogram in Figure 6B shows a significant proportion of embryos with positive gradient tail slope. To test whether this is an artifact of our image analysis procedure, in particular of the normalization by the nuclear intensity, the following control simulations were done. The average non-uniformity in the nuclear intensity from our dataset was calculated. The average non-uniformity had a peak value of 162% of the median nuclear intensity, and a minimum value of 72.79% of the median nuclear intensity. This non-uniformity was modeled as a circular normal distribution with a concentration parameter of 8.16 (red curve, Fig S4C). We normalized a Gaussian-like curve, with flat gradient tails (blue curve in Fig S4C), by this non-

uniform nuclear intensity, resulting in the green curve in Fig. S4C. The green curve was then subjected to the same fitting procedure as our real data, and the normalized slope of the gradient tail was found. This procedure was performed N = 160 times, each with a random placement of the location of the peak in the nuclear intensity (DV position = 0.28 in the example shown in Fig. S4C, red curve). This resulted in the histogram of normalized gradient tail slopes found in Fig. S4E. The results show that the histogram has a slightly positive bias, but is mostly evenly distributed around zero. This is markedly different from the histogram in Fig 6B, and this control simulation procedure shows the gradient tail slopes calculated from our fixed embryo data are not an artifact of the image analysis procedure.

Measuring gene expression profiles

To obtain semi-quantitative data of the location of gene expression (that is, data that contains relative intensities, but not absolute intensities), first the ventral midlines of the fixed embryos in Figures 4-7 were found manually. Next, each gene expression profile was background-subtracted and normalized for laser power (see below). Then, assuming symmetry about the ventral midline, each gene expression profile was split into two, corresponding to the right and left sides of the embryo. Finally, gene expression profiles for each nuclear cycle or nuclear cycle substage were averaged together.

The locations of the gene expression boundaries, as found in Figure 7I,L,O, were quantified as described previously (Liberman et al., 2009). Briefly, the gene expression pattern for each gene in each embryo was fitted to "canonical" gene expression patterns based on changing the heights, widths, and locations of the canonical patterns. Once best-fit canonical

gene expression patterns were found, gene expression boundary locations were defined as the locations where the canonical pattern reached half-maximal intensity.

Analysis of intronic sog

For intronic *sog*, the intensity of the nuclear dots (nascent transcripts) was found in the following manner. First, in the intronic *sog* color channel, the max intensity pixel in each nucleus was found. To ensure this pixel was not the effect of a single improbable photon, the median intensity of the 3-by-3 neighborhood centered on this pixel was taken as the intensity of the nuclear dot.

Because the profiles of nascent transcripts are salt-and-pepper (see Fig. S3F), this was translated into a smooth profile in the following manner. First, the locations of the nuclei (in normalized DV coordinates) were placed into bins on a mesh from zero to one with 40 points. The value of the non-smoothed profile at bin *i* was taken as the max intensity seen in a window 5 bins wide, centered at bin *i*. If a bin contained zero nuclei, this mesh point was given a value corresponding to the average of the two intensities at the nearest two mesh points with at least one nucleus, with the provision that the two mesh points had to be on different sides of the point with zero nuclei. In other words, go left until you find a mesh point with a value, and then right until you find one with a value, and take the average of those two.

This procedure will clearly give you a profile that is too broad, so to narrow it back down to the correct size, we morphologically eroded the profile with a structuring element of width 5 points (to counteract the previous sliding window of width 5 points). After this procedure, the non-smoothed profiles were smoothed using a sliding window of width 5 points (an averaging procedure).

Background subtraction of gene expression profiles and Sna-GFP profiles

A precise, quantitative background is difficult to measure on embryos that have been manually cross sectioned. This is because the optical section taken using confocal microscopy must pass through varying thicknesses of physically-damaged tissue. However, a rough estimate of the background intensity of fluorescent *in situ* hybridization images was determined in the following manner. First, control wildtype embryos were taken through the fluorescent *in situ* hybridization protocol, but no anti-sense riboprobes were added. However, the primary and secondary antibodies were used consistently. For example, for *sna*, the hapten used with the anti-sense riboprobe was biotin, with anti-biotin raised in goat as primary antibody, and anti-goat (raised in donkey) conjugated with Alexa Fluor 488 was used as secondary antibody. Therefore, the background experiment for *sna* included embryos treated with those two antibodies. n = 8 (for *sog*, *zen*) or n = 16 (for *vnd*, *sna*) of these embryos were imaged, using the same microscope conditions as were used for experimental embryos, with the exception of changing laser power (see below). Intensity profiles from these images were found using the same image analysis procedure as for the experimental embryos. The average background intensity profiles are plotted in gray in Fig. S2A, with errorbars representing the standard deviation of all background intensity profiles for that gene.

Once background intensity profiles were found, they were applied to the experimental data in the following manner. The "structural background" of each gene expression intensity profile was found through a morphological opening using an appropriately large structuring element (for Type III genes, 60% of the embryo perimeter; for others, 40% of the embryo perimeter). This structural background can be thought of as the intensity of the profile outside of its normally-accepted expression domain. For example, with *sna*, this would roughly be the

intensity of the profile from DV position = 0.20 to 1. If this structural background was statistically greater than the background intensity from the control embryos, then the background from the control embryos was used. If not, then the structural background was used (in which cases the structural background is likely to correspond to a true lack of gene expression). This is because of the uncertainty in comparing embryo-to-embryo when sectioning manually can sometimes lead to structural backgrounds less than the background from control embryos.

The background-subtracted (and normalized; see below) profiles were plotted in Fig. 4F, and were also used in the fitting procedure for the mRNA dynamics model (see below).

For Sna-GFP, a similar procedure was used, with the control embryos being wildtype (that lack Sna-GFP).

Correction for laser power

To correct for embryos imaged on different days, laser power baselines for each day were taken during each imaging session. Using those data, gene expression profiles, as well as Sna-GFP profiles, were normalized according to the laser power used to image them (Liberman et al., 2009). This also allowed us to capture a full dynamic range for embryos with drastically different intensities (such as control embryos or early embryos that contained no gene expression vs. embryos displaying bright, "mature" gene expression profiles).

Normalization of gene expression profiles

In addition to being background-subtracted and laser power corrected, the gene expression profiles of *sna*, s*og*, *vnd*, and *zen* shown in Fig. 4F (and also used for data-fitting; see below) were normalized such that the peak intensity was equal to one. This was done in the

following manner. After average profiles were found for each gene and each nuclear cycle substage, they were background subtracted. Then, for each gene, the peak intensity across all nuclear cycle substages was set to one. For example, for *sna*, the peak intensity for all nuclear cycle substages occurred during late nc 14 at roughly x = 0.05 (see Fig. 4F). All of the averaged *sna* profiles (across all nuclear cycle substages) were then divided by this intensity.

Averaging of the three live Dorsal-Venus nuclear gradient time series

The three live Dorsal-Venus nuclear gradient time series (Fig. S1B-D) were averaged together in the following manner. Each nuclear cycle interphase was treated independently, as was each nuclear cycle mitosis. As an example, the length of nc 11 interphase from each embryo was determined based on the "saw-tooth" pattern of the gradient amplitude. Due to small variations in development time, these lengths were slightly different. The gradient amplitudes, basal levels, and widths during nc 11 interphase were plotted together after stretching or shrinking the duration of nc 11 interphase of each individual embryo to fit the average duration of nc 11 interphase (Fig S1F-H). This same stretching/shrinking/averaging procedure was performed on each interphase and mitosis. Afterwards, the gradient amplitudes, basal levels, and the gradient widths were averaged together to arrive at an averaged Dorsal-Venus nuclear gradient (black curves in Fig. S1F-H). The background levels (gray curve with errorbars in Fig. S1B-D,G) were measured from embryos carrying only H2A-RFP (and not Dorsal-Venus) that were imaged in the same manner as the embryos in Fig. S1B-D.

Simulation of the Dorsal gradient

An estimate of the wildtype Dorsal gradient was constructed from live imaging time series data of Dorsal-Venus and nc 14 fixed tissue data in the following manner. The averaged gradient amplitude and basal levels from live Dorsal-Venus data (see above) were used as $A(t)$ and $B(t)$. Due to the fact that the Dorsal-Venus nuclear gradient is measurably wider than the wildtype Dorsal nuclear gradient (Fig. 1D-F), and that live imaging showed the gradient width to be constant in time, the width was taken to be 0.14, the mean of the nc 14 fixed tissue data set (Figs. 1F and 6A). The slope of the gradient tail was assumed to be equal to $M(t) = -0.1A(t)$ to reflect the mean value of the normalized slope of the gradient tail. After $A(t)$, $B(t)$, σ, and $M(t)$ were computed, the simulated wildtype Dorsal nuclear gradient was computed according to Eqn. 2, with 10% Gaussian noise added to each point in space and time. For example, the noise added to the gradient $c(x,t)$ at $x = x_0$ and $t = t_0$ was randomly chosen from a normal distribution with mean $c(x_0,t_0)$ and standard deviation $c(x_0,t_0)/10$. The rationale for including noise in the Dorsal gradient is because without relevant biological noise, a deterministic model can read an arbitrarily shallow slope with perfect precision. A level of 10% noise was chosen as suggested by previous studies of morphogen gradient precision (Gregor et al., 2007a). For an exploration of the effect of this noise on gene expression patterns, see Fig S5.

Statistical analyses

The widths of some pairings of the populations of embryos in Fig. 1F were shown to have statistically different means by either modified *t*-test (Welch, 1947) for differences between

wildtype cross sections and anti-Dorsal stainings of *dl1/+; dl-venus/+*, or by *t*-test for correlated samples for differences between anti-Dorsal and anti-GFP within the same embryos.

Time delays of mRNA production

The four genes analyzed here (*sna*, *vnd*, *sog*, *zen*) have gene lengths of 1676, 6780, 21970, and 1330 bp, respectively. At a transcription rate of 1.1 kb/min (Thummel et al., 1990), this would mean time delays of 1.52, 6.16, 19.97, and 1.21 minutes, respectively. At nearly 20 minutes for *sog*, we would not expect *sog* expression before mid nc 14, as unfinished transcripts are not "carried over" through mitosis into the next nc interphase, but are instead degraded (Rothe et al., 1992; Shermoen and O'Farrell, 1991). Even the fastest reported transcription rate for the early embryo (1.4 kb/min, Shermoen and O'Farrell, 1991) would result in a delay of almost 16 minutes for *sog*, which again is prohibitively long for the appearance of mature *sog* transcripts before mid nc 14. Since *sog* transcripts were seen in most of the embryos from late nc 13, for our model we assumed the transcription rate for all genes was fast enough such that *sog* would be just completed half way through nc 13 interphase (6.15 min, corresponding to 3.5 kb/min). While this may be a questionable assumption, it is consistent with the earlier than otherwise expected appearance of *sog* transcript.

Staging of fixed embryos

Nuclear cycle 13 was divided equally into early and late substages. nc 14 lasts around 45 minutes at 25ºC and was thus separated into three different substages based on nuclear morphology: early, mid, and late. Comparing the nuclear morphology of fixed, cross-section embryos with that of H2A-RFP in live embryos, it was determined that the binning procedure

resulted in the early and late nc 14 stages being ~10 minutes in duration or ~20% of nc 14. Mid nc 14 was the longest at ~30 minutes or ~60% of nc 14.

Fitting model parameters to gene expression data

The semi-automated fitting procedure took place as follows. First, for *sna*, the model parameters θ_{sna} (the Dorsal signaling threshold to activate *sna* gene expression) and τ_{sna} (the lifetime of *sna* gene product) were optimized against gene expression data for *sna*, depicted in Figure 4F.

The initial guess for the value of the threshold θ_{sna} corresponded to the value of the simulated Dorsal levels at $x = 0.20$ at a timepoint when the gradient amplitude was maximal in nc 14. Allowing for 20% error in this presumptive gene expression boundary (that is, x between 0.16 and 0.24), upper and lower bounds on the possible value of θ_{sna} were chosen. Because the threshold corresponded to a binary switch, a fitting procedure for this parameter using Newton's method on the gradient of the objective function was inherently unstable. Therefore, thirty values of the threshold were chosen (with a uniform distribution between the upper and lower bounds), and fifty values of mRNA lifetime were chosen (uniformly-distributed on a log scale between 1 and 1000 minutes).

The objective function γ was a chi-square function:

$$\gamma = \sum_{i=1}^{N} \frac{(Y_i - \hat{y}_i)^2}{\sigma_i^2},$$

where N=151 was the number of points along the discretized DV coordinate; Y_i was the background-subtracted, normalized average value of the measured gene expression profile at x_i;

$\hat{y}_i$ was the value of the simulated gene expression profile for the current choice of θ_{sna}, τ_{sna} at x_i; and σ_i was the standard error of the mean for the measured gene expression profiles at x_i.

For each choice of fixed (θ_{sna}, τ_{sna}), a value γ was calculated. The choice of (θ_{sna} , τ_{sna}) that resulted in the smallest value of γ was taken as the best-fit parameters for *sna*.

Once the optimum values for θ_{sna} and τ_{sna} were found, the same optimization procedure was performed to determine (θ_{vnd}, τ_{vnd}) and (θ_{sog}, τ_{sog}) independently. However, the optimization procedure was unstable for these genes in that the program did not converge on the best-fit mRNA lifetime. Therefore, the parameters were manually adjusted "by-eye" such that simulated gene expression matched the *vnd* and *sog* patterns in late nc 13 through late nc 14.

The same optimization procedure was performed on the equation for *zen*, with the exception that only observed data from late nc 13 and early nc 14 were used to fit the parameters, because by mid nc 14, the Dpp-dependent expression of *zen* was already quite pronounced.

The final outputs of the fitting procedure showed mRNA lifetimes to be 12 minutes for *sna*, 10 minutes for *sog*, 10 minutes for *vnd*, and 12 minutes for *zen*.

zen repression of sog

For Fig. S5, a case was considered in which a dorsally-acting factor repressed *sog*. This was motivated by the fact that, if the *sog* threshold was too low, *sog* was expressed strongly in all nuclei (except those in which it is repressed by *sna*), and if the threshold was made only slightly higher, the domain of *sog* expression became too narrow. This implies that there may be a dorsally-acting factor that represses *sog*. In this case, we allowed *zen* to repress *sog* strongly in the same manner that *sna* repressed *sog* ventrally, with $K_{zen} = 0.05$.

Supplemental References

Kosman, D., Mizutani, C.M., Lemons, D., Cox, W.G., McGinnis, W., and Bier, E. (2004). Multiplex detection of RNA expression in Drosophila embryos. Science *305*, 846.

Otsu, N. (1979). A Threshold Selection Method from Gray-Level Histograms. Systems, Man and Cybernetics, IEEE Transactions on *9*, 62-66.

Welch, B.L. (1947). THE GENERALIZATION OF 'STUDENT'S' PROBLEM WHEN SEVERAL DIFFERENT POPULATION VARIANCES ARE INVOLVED. Biometrika *34*, 28-35.